Temporal Design of Flow Intermittency in Grooved Channel for Advanced Heat Transfer Enhancement

Zhihan Zhang [(1)], Qiang Zhang [(1,2)] , Zhaoguang Wang [(1)] *

[(1)] University of Michigan – Shanghai Jiao Tong University Joint Institute, Shanghai Jiao Tong University, Shanghai, China

[(2)] City, University of London, London, UK

* Corresponding author: zhaoguang.wang@sjtu.edu.cn

Abstract

The present numerical work is a continuing exploration of heat transfer enhancement by flow intermittency in grooved channels based on the energy buffer mechanism elucidated in our previous study, and aims to quantitatively optimize the time domain design of the intermittency pattern. The open-source computational fluid dynamics code OpenFOAM is employed to resolve the intermittent channel flow with triangular surface grooves. The main conclusion is that the optimal thermal performance is achieved when the time duration of each intermittency stage (acceleration, pulse-on, and deceleration) matches the characteristic time of flow dynamics (vortex development and heat transportation). The averaged surface Nusselt number is increased by 120% under the optimized intermittency pattern with the thermal performance factor reaching 1.9. The pulse-off stage of the flow intermittency expands further flexibility to meet diverse prerequisites in practical applications (constant coolant consumption, energy cost, or cooling capacity). By revealing the characteristic flow physics that governs the thermal performance of intermittent flow in grooved channels, the present work novelly proposes quantitative guidance on the temporal design of flow intermittency to achieve effective heat transfer enhancement.

Keywords: intermittent flow, vortex development, heat transportation, grooved channel, heat transfer enhancement

Nomenclature

Roman symbols		Greek symbols	
Nu	Nusselt number	Δ	Relative difference between steady and unsteady results, (%)
Pr	Prandtl number	α	Thermal diffusivity, ($m^2 \cdot s^{-1}$)
Re	Reynolds number	β	Thermal expansion coefficient, (K^{-1})
Ri	Richardson number	γ	Close time ratio, $\frac{\text{close time}}{\text{intermittent period}}$
St	Strouhal number	η	Thermal performance factor
C_p	Fluid specific heat, ($J \cdot kg^{-1}K^{-1}$)	ν	Kinematic viscosity, (Pa•s)
D_H	Hydraulic diameter, (m)	ρ	Density, ($kg \cdot m^{-3}$)
F	Intermittent frequency, (Hz)	ω_z	Z-direction vorticity, (s^{-1})
f	Average Fanning friction factor,	Superscript	
g	Acceleration of gravity, ($m \cdot s^{-2}$)	$\overline{(\cdot)}$	Area-averaged value
H	Channel height, (m)	*	Dimensionless form
h	Heat transfer coefficient, ($W \cdot m^{-2} \cdot K^{-1}$)	Subscripts	
k	Thermal conductivity, ($W \cdot m^{-1} \cdot K^{-1}$)	a	Acceleration stage
l	Groove depth, (m)	b	Bulk-averaged value
p	Pressure, (Pa)	d	Deceleration stage
q	Heat flux, ($W \cdot m^{-2}$)	m	Time-averaged value
t	Flow time, (s)	o	Pulse-off stage
T	Temperature, (K)	p	Pulse-on stage
U	Velocity of inlet flow, ($m \cdot s^{-1}$)	s	Steady value

1. Introduction

Driven by the ever-growing heat load in industrial applications such as high-performance processors and battery energy storage systems, efficient thermal management urges for advanced cooling technologies. Liquid cooling has been widely employed in industrial applications for thermal management of electronics, electrical vehicle batteries, fuel cells and energy storage systems. The rapid increase of heat load in these applications demands more effective and efficient cooling designs. In practice, many cooling scenarios involve laminar channel flow, where heat transfer enhancement techniques under steady flow conditions have been well studied and most are related to area increase by various surface structure designs.

Adding groove structures to the heating surface is a widely used passive technique to enhance thermal performance. Groove shapes and dimensions are critical parameters that determine the heat transfer enhancement and accompanying pressure loss [1, 2]. Different groove geometries including dimples [3] and triangular shapes [4] have been studied extensively, and various optimization methods [5] have been reported. Although remarkable improvement of the overall thermal performance is achieved (80% improvement reported by Xia et al. [6]), heat transfer inside the grooves remains poor due to the inevitably produced cavity vortices.

Flow pulsation has been studied in a considerable amount of literature as an active flow control technique for heat transfer enhancement. However, the conclusions on the thermal performance in pulsating flow remain inconsistent. The influence of flow unsteadiness on heat convection was shown to be positive [7, 8], negative [9, 10], or marginal [11, 12], highly depending on the choice of pulsation frequency and amplitude as well as the boundary layer development [13].

In recent years, the combination of pulsating flow and surface structures has gained increasing attention. Most of the published studies focused on sinusoidal pulsation profiles. Jin et al. [14] experimentally explored the thermal performance of a

single-sided triangularly grooved channel. A maximum of 350% heat transfer enhancement was achieved at pulsation amplitude A = 0.5, Reynolds number Re =270, and Strouhal number St = 0.34. The enhancement decreased with the Reynolds number increasing. Zontul et al. [15] conducted similar experiments in a rectangular grooved channel and attributed the 90%-140% thermal performance improvement to flow mixing and groove-mainstream interaction. Further analyses by Zontul and Şahin [16] revealed that the enhancement depended on the pulsation frequency and was more profound at low Reynolds numbers. Jafari et al. [17] adopted the Lattice Boltzmann Method to investigate the heat transfer of a corrugated channel with sinusoidal pulsating flow under laminar conditions. The heat transfer rate was linearly proportional to the pulsation amplitude under constant frequency and a maximum enhancement of 20% was achieved with the highest pulsation amplitude A = 0.25 at Re =150 and St = 0.25. A numerical analysis of pulsating flow in a periodically corrugated channel with discrete V-type winglets was conducted by Akcay [18]. The highest thermal performance factor η of 5.74 was reported at Re =1000 and St = 8, and the corresponding Nusselt number was increased by 8 times. Muñoz-Cámara et al. [19] carried out experimental research on pulsating laminar flow in a circular duct with perforated baffles. The resultant heat transfer was improved maximally by five times. Habibi et al. [20] numerically investigated pulsating flow in a twisted pipe at laminar condition. It was concluded that the flow pulsation exerted stronger effects on heat transfer for regions covered by vortex bubbles. Hoang et al. [21] numerically studied the heat transfer of a V-sharp waveform channel under pulsating conditions using large-eddy simulation (LES) method. The thermal performance factor was improved by the enhanced flow instability, and reached 1.3 to 1.4 compared with 0.9 to 1.17 under steady condition (pulsating amplitude $A \leqslant 1.0$, $0 \leqslant St \leqslant 0.79$, and $2000 \leqslant Re \leqslant 6000$). Kurtulmuş and Sahin [22] reported experimental work on turbulent pulsating flow in a sinusoidal wavy channel. The highest thermal performance factor was 1.46 at Re =4000 and St = 1.03. Similar conclusion was drawn by Jin et al. [14] that an optimal Strouhal number existed to achieve the highest heat transfer enhancement.

Grooved channel flow with other pulsating profiles such as triangular and square waveforms were studied less extensively, despite potentially higher heat transfer augmentation. Mehta and Khandekar [23] experimentally explored heat transfer of laminar thermally-developing flow in a square mini channel with square-wave velocity profile. Only marginal enhancement (less than 5%) was reported under the studied conditions (Womersley number $0.8 < Wo < 5.9$). Bayomy and Saghir [24] both numerically and experimentally investigated the thermal performance of aluminum foam heat sink subjected to a square-wave pulsation. The average Nusselt number enhancement was 14% with the pulsation amplitude of Reynolds number and pulsation frequency ranging between 300 and 1350, 0.04 Hz and 0.1 Hz respectively. Wang et al. [25] numerically studied the laminar heat convection in a louvered microchannel heat sink with Lattice Boltzmann Method under triangular-wave pulsation. The highest thermal performance factor reached 1.7 at $St = 1.5$ and was ascribed to the promoted mixing effects by a series of vortex expansion and contraction under pulsation ($100 < Re < 300$, pitch ratio of 0.58). Xu et al. [26] conducted experiments of a micro channel heat sink with flow pulsation of different waveforms and concluded that the square-wave pulsation yielded the highest heat transfer enhancement. Chang and Cheng [27] experimentally compared heat transfer in a channel flow with hybrid pin-fin array under pulsation conditions ($1{,}500 < Re < 20{,}000$, $0.00028 < St < 0.017$). The increase of vent period from 1/4 to 3/4 pulsating cycle led to the decrease of relative Nusselt number and increase of relative friction factor, with the corresponding thermal performance factor reduced from 2.8 to 2.3.

Different from conventional pulsation patterns, intermittent flow adds another characteristic design parameter to the flow unsteadiness, i.e., pulse-off time. Flow intermittency has shown superior performance to sinusoidal pulsations in enhancing impingement heat transfer [28, 29]. In particular, Zhang et al. [30] reported a remarkable enhancement in jet cooling efficiency with the high-amplitude intermittent flow at large close time ratios. The allowable stop off time provided by solid heat conduction was thoroughly discussed as well. However, the influence of flow intermittency on channel flow heat transfer is seldom studied. Very recently, Zhang et

al. [31] reported notable heat transfer enhancement in a grooved channel by adopting intermittent flow with high amplitudes and large close time ratios, and proposed the energy buffer mechanism that governed the vortical flow field.

Based on the understandings of the energy buffer mechanism revealed in the previous study [31], the present work numerically compares the thermal performance of grooved cooling channels at different intermittent velocity profiles, and highlights the individual effect of each characteristic time (duration of flow acceleration, pulse-on, deceleration and pulse-off stages) on the heat transfer enhancement. Special effort is paid to illustrate the criticality of matching the time scales between the dynamic vortex evolution and the flow intermittency pattern. The novelty of the present work lies in the reveal of flow features that play a decisive role in heat transfer enhancement and the demonstration of quantitative criteria that guide the temporal design of flow intermittency.

2. CFD methods and validation

The present work employs a 2-D computational domain that refers to the methodology adopted in previous studies [18, 32], considering that the dominant flow features in the cooling channel evolve along the streamwise direction instead of the spanwise direction. The 2-D computational domain is shown in Fig. 1 and comprises a corrugated channel with 10 aligned triangular grooves on both sides. The channel height H is 0.0025 m and the corresponding hydraulic diameter D_H equals 0.005 m. The smooth area upstream of the grooved region is $50D_H$ long to eliminate the entry flow effect [33], and the downstream outlet is $6D_H$ away from the last grooves to avoid the occurrence of backflow [18]. The triangular groove geometries are adapted from Eiamsa-ard and Promvonge [33] and Zhu et al. [34] and detailed dimensions are provided in Fig. 1. The current numerical work adopts structured mesh with dense grids refined near wall surfaces and inside grooves to accurately capture boundary layer features and dynamic vortical structures.

The channel inlet is specified with spatially uniform velocity and constant temperature T_{in} of 293.15 K. The outlet is assigned a preset pressure of 1 bar. The grooved regions of the channel surface have a constant heat influx q of 20000 W/m^2 and other smooth regions are regarded as adiabatic boundaries. The coolant in the present work is water with a Prandtl number of 7.02. Based on the evaluation of the Richardson number in the following Eqn. (6), the effect of natural convection is negligible in the current setup. The coolant is considered to be incompressible, single-phase, and Newtonian-type with constant thermophysical properties. The effects of gravity and heat radiation are neglected. Based on these assumptions, the governing equations of the transient laminar flow problem are as follows:

Continuity equation:

$$\nabla \cdot U = 0 \tag{1}$$

Momentum equation:

$$\frac{DU}{Dt} = -\frac{1}{\rho}\nabla p + \nu \nabla^2 U \tag{2}$$

Energy equation:

$$\frac{DT}{Dt} = \alpha \nabla^2 T \tag{3}$$

Here, U, T, p, ρ, ν, α, and t are the flow velocity, temperature, pressure, density, kinematic viscosity, thermal diffusivity and time, respectively.

In the present work, the time-varying Reynolds number Re is calculated as

$$Re = \frac{UD_H}{\nu} \tag{4}$$

The time-averaged Reynolds number is:

$$Re_m = \frac{\int_0^{t_{cycle}} Re \, \mathrm{d}t}{t_{cycle}} \tag{5}$$

The time-averaged Reynolds number Re_m is maintained at 100 for all cases, ensuring that the overall coolant consumption stays identical. The peak Reynolds number through one intermittency cycle is constrained at $10Re_m$ (i.e., 1000) and thus the flow condition remains laminar during the entire period.

The Richardson number Ri is calculated as:

$$Ri = \left(\frac{g\beta\Delta T H^3}{\nu^2}\right) / Re_{\mathrm{m}}^2 = 0.094 \ll 1 \tag{4}$$

with g and β being the acceleration of gravity 9.8 m/s^2 and the thermal expansion coefficient 2.1e-4 K^{-1}, respectively.

In the present work, to more thoroughly explore the individual effect of each stage in the intermittency pattern (flow acceleration, pulse-on, deceleration and pulse-off), the following dimensionless time is defined:

$$t^* = \frac{tU_m}{l} \tag{7}$$

The groove depth l is chosen as the reference length scale, because the main flow features arise from the evolution of cavity vortex of which the size and the growth time are determined by the groove depth. The dimensionless times corresponding to the four stages of one intermittency cycle are labeled in Fig. 2., with the subscripts 'a', 'p', 'd', and 'o' representing the acceleration, pulse-on, deceleration, and pulse-off stages respectively.

The present numerical study was performed with the open-source CFD code OpenFOAM (Ref. Weller et al. [35]). The unsteady laminar flow problem was initialized with steady-state results and solved by the PISO algorithm. The Courant number for the transient calculation was controlled below 0.3 to accurately capture the temporal development of vortical flow structures.

Both the grid independency study and numerical model validation have been provided in the previous study [31]. A mesh size of 34 k grids well satisfies the requirement of grid convergence and the present computational setup gives reliable results that agree well with both analytical solution [36] and experimental measurement [37] published in previous literature.

In the current work, the Nusselt number Nu is defined as:

$$Nu = \frac{q}{(T - T_b)} \cdot \frac{D_H}{k} \tag{8}$$

with k representing the fluid thermal conductivity. Here, the flow bulk temperature T_b along the streamwise direction serves as the reference temperature and is formulated as:

$$T_b = T_{in} + \frac{2qx}{U_m H \rho C_p} \tag{9}$$

where x is the streamwise distance from the starting location of the heated region and C_p is the coolant specific heat. The time-averaged Nusselt number is calculated as:

$$Nu_m = \frac{\int_0^{t_{cycle}} Nu \, \mathrm{d}t}{t_{cycle}} \tag{10}$$

The dimensionless temperature T^* is defined as:

$$T^* = (T - T_{in})/(T_{out} - T_{in}) \tag{11}$$

Here, T_{out} is the mass-averaged outlet temperature.

The pressure loss over the grooved region is quantified by the apparent friction factor f, referring to the published studies [17, 21]:

$$f = \frac{(p_1 - p_2)D_H}{2\rho L U_m^2} \tag{12}$$

with p_1 and p_2 representing the area-averaged static pressure at upstream and downstream cross section of the grooved region and L the grooved length. The time-averaged friction factor is formulated as:

$$f_m = \frac{\int_0^{t_{cycle}} f \, \mathrm{d}t}{t_{cycle}} \tag{13}$$

The overall thermal performance is evaluated with the thermal performance factor η which is also known as thermal enhancement efficiency. This concept was firstly proposed by Webb [38] and is adopted in the present study to quantify the improvement of intermittent cases relative to steady cases regarding both heat transfer enhancement and pressure loss penalty. Here, η is calculated as:

$$\eta = \left(\frac{Nu_m}{Nu_s}\right) \cdot \left(\frac{f_m}{f_s}\right)^{-\frac{1}{3}} \tag{14}$$

The subscript m and s represent time-averaged values for intermittent cases and values for steady cases, respectively. The same formulation was adopted by Zontul and Sahin [16] and Ackay [18] to quantify the heat transfer performance in a 2D channel with surface grooves of different shapes.

3. Results and Discussion

The flow physics that governs the remarkable heat transfer enhancement in the grooved cooling channel by high-amplitude intermittent flow has been successfully explained by the energy buffer mechanism proposed in our previous study [31]. Figure 3 reviews the essential vortical flow structures inside the cooling channel at different intermittency stages. During the pulse-on stage, flow separation occurs at the groove leeward surface and leads to the formation of cavity vortices that occupy the grooves. The subsequent deceleration stage induces strong adverse pressure gradient along the channel and causes the cavity vortices to swell up significantly. During the pulse-off period, the enlarged vortices detach from the channel wall, rolling a great amount of hot fluid off the heating surface. Meanwhile, intense near-wall reverse flow is induced by the extensive flow recirculation above the grooves. Such reverse flow sweeps over the heating surface at similar velocity magnitudes to the time-averaged flow rate, significantly promoting the local heat convection despite no coolant inflow. At the arrival of the subsequent flow pulse, the hot fluids that are entrained into the recirculating zone are vented out of the channel. In such a way, the cavity vortices inside the grooves absorb energy from the mainstream deceleration and release the energy by driving strong flow recirculation during the pulse-off stage, serving as energy buffers over the intermittency cycles.

On the basis of the energy buffer mechanism, the present work details the flow evolution at each intermittency stage and further correlates the intermittency durations with the flow characteristic times to achieve optimal thermal performance. It is worth re-emphasizing that the time-averaged coolant flow rate and the intermittency amplitude remain identical for all cases in the current work. All the time-averaged variables are averaged over a full intermittency cycle including the pulse-off stage.

Acceleration Stage and Pulse-on Stage

During the acceleration and pulse-on stages, the dominant flow feature in the

cooling channel is the development of cavity vortices inside the grooves. Figure 4 compares the cavity vortex morphology and the vorticity strength at the pulse end among cases with different pulse-on durations. The flow separation is initiated at the groove leeward surface and gradually expands towards the windward side. When t_p^* = 0.36, the separation region occupies the entire groove and the cavity vortex reaches the full size. As the pulse-on duration is further extended, the cavity vortex morphology remains nearly unchanged but the area-averaged vorticity strength decays continuously towards the steady state.

The cavity vortex which acts as the working medium in the energy buffer mechanism greatly affects the intensity of the recirculating flow motion and thus the thermal performance in the subsequent stages. Figure 5 compares the flow recirculation velocity and the temperature distribution at the pulse-off stage for three cases with different pulse-on durations. The shown time instant is at one tenth of the pulse-off period. For the case with t_p^* = 0.36, the cavity vortex develops to the full morphology at the end of the pulse-on stage (in Fig. 4) and further evolves into extensive recirculating zones at the pulse-off stage (in Fig. 5) after absorbing energy from the mainstream deceleration process. The intense flow recirculation induces near-wall reverse flow that notably exceeds the time-averaged velocity of the coolant inflow and draws a considerable amount of hot fluid out of the groove, therefore enhancing the local heat convection by both promoting the heat transfer coefficient and enlarging the driving force (i.e., temperature difference). For the case with t_p^* = 0.06, since the cavity vortex development is insufficient over the short pulse-on period, the resultant recirculating zone at the pulse-off stage is constrained close to the groove leeward surface. Consequently, the enhancement of the near-wall flow motion and the redistribution of the in-groove hot fluid are significantly less profound compared to the case with t_p^* = 0.36. For t_p^* = 3.96, the overlong pulse-on stage causes the fully developed cavity vortex wearing off and the correspondingly lengthy pulse-off stage (to maintain the same time-averaged coolant flow rate) also dissipates the recirculating flow motion. As shown in Fig. 5, the recirculating zone drifts away from the heating surface, exerting marginal effects on the near-wall velocity and temperature

distributions.

Figure 6 quantitatively compares the spatial variation of time-averaged Nusselt number among cases with different pulse-on durations. Remarkable heat transfer enhancement is obtained by adopting the intermittent flow, especially for groove surfaces that suffer poor cooling performance in conventional steady flow. This agrees with the flow features reported in Fig. 5 that the hot fluid accumulated inside the groove is entrained off the boundary by the extensive flow recirculation. The improvement of the thermal performance becomes optimal at $t_p^* = 0.36$, with the local increase of Nu_m reaching 175% and the averaged increase exceeding 75% compared to the steady-flow value. This optimal pulse-on duration is consistent with the time for the cavity vortex to fully develop as demonstrated in Fig. 4.

As for the acceleration stage, the dominant flow feature is the cavity vortex development as well. Therefore, the influence of the acceleration duration on the cavity vortex strength and on the heat transfer enhancement resembles that of the pulse-on duration. As demonstrated in Fig. 7, for cases with t_p^* maintained at 0.16, t_a^* shorter than 0.6 leads to an underdeveloped cavity vortex while longer t_a^* causes extra dissipation of the vortex strength and results in further reduction of the area-averaged vorticity magnitude. The respective consequence on the recirculating flow motion and on the temperature field redistribution at the subsequent pulse-off stage is similar to the results presented in Fig. 5 and omitted here for brevity.

Figure 8 compares the variation of the averaged Nusselt number, the friction factor and the overall thermal performance factor for cases with different acceleration and pulse-on durations. Although the heat transfer enhancement by flow intermittency is accompanied by additional pressure loss, the maximum improvement of the overall thermal performance factor achieves 1.5 times of the steady-flow value. It is noteworthy in Fig. 8(b) that the highest Nusselt number and the highest friction factor appear at different acceleration durations. This is attributed to the decoupling between hydrodynamic and thermal boundary layer development in the intermittent flow. In particular, while no net inflow exists during the pulse-off period (consequently no pressure loss), the local flow recirculation inside the channel still sustains heat

convection of a certain intensity as illustrated in Fig. 3.

The optimal conditions in Fig. 8 correspond to cases where the cavity vortex fully develops to occupy the entire groove, which agrees with the flow structure analyses in Fig. 4-7. Therefore, the combination of acceleration and pulse-on durations in practical designs of flow intermittency needs to match the characteristic time of the cavity vortex development.

Deceleration Stage

At the flow deceleration stage, strong adverse pressure gradient is induced along the channel, causing the cavity vortex to swell up significantly. As the cavity vortex evolves into a recirculating zone detached from the boundary, a layer of near-wall reverse flow is developed. Figure 9 compares the recirculating flow structures at the deceleration end among cases with different deceleration durations. The three cases show qualitatively similar flow patterns because they share identical fully-developed cavity vortices after equally long acceleration and pulse-on stages. But longer deceleration duration allows the recirculation zone to detach itself further away from the boundary, resulting in the near-wall flow recirculation being more extensive yet less intense. The heat transfer analyses in the later Fig. 11 reveal that $t_d^* = 0.44$ greatly outperforms both $t_d^* = 0.04$ (with the most intense recirculation) and $t_d^* = 0.80$ (with the most extensive recirculation), indicating that neither the intensity nor the range of the recirculating zone dominates the thermal performance as far as the cavity vortex achieves full development through the acceleration and pulse-on stages.

Another distinctive flow feature affected by the deceleration duration is the heat transportation along the channel. As previously demonstrated in Fig. 3, the recirculating flow motion at the pulse-off stage drags the near-wall hot fluids off the boundary and entrains them into the detached recirculation zone. The hot-fluid core dwells above the groove with a stem connected to the wall surface until being transported downstream by the succeeding intermittent flow motion. Such transportation is initiated at the acceleration stage and ended at the deceleration stage, as presented in Fig. 10. The parameters S_{ta*}, S_{tp*} and S_{td*} represent the travel distance of the off-wall hot fluids

through the acceleration, pulse-on and deceleration stages, respectively. Since the acceleration and pulse-on durations are kept identical for the three cases in Fig. 10 to yield fully-developed cavity vortices, the difference in the overall transportation distance is governed by the deceleration duration. For $t_d^* = 0.04$, the hot-fluid core travels across one groove pitch with its form preserved, while the hot-fluid stem is rolled into the groove by the newly developed recirculating flow. Similar flow patterns are observed for $t_d^* = 0.80$ where the hot-fluid core is transported over approximately two groove pitches. For $t_d^* = 0.44$ with a transportation distance of 1.5 groove pitches, however, the inter-core coolant instead of the hot-fluid stem is drawn towards the groove surface and effectively cools the wall surface. This explains the superior thermal performance of $t_d^* = 0.44$ over other deceleration durations.

Figure 11 presents the spatial distribution of the time-averaged Nusselt number for cases with different deceleration durations. As explained by the hypothesis of effective transportation distance, the optimal heat transfer enhancement is observed at $t_d^* = 0.44$ with the local improvement of Nu_m exceeding 200% and the averaged enhancement reaching 115% in comparison to the steady-flow value. Figure 12 summarizes the variation of the averaged Nusselt number, the friction factor as well as the overall thermal performance factor with the deceleration duration. Different from the bell-shaped distribution of the thermal performance, the pressure loss drops consistently as the deceleration duration is prolonged. This again clearly demonstrates the decoupling between the hydrodynamic and thermal boundary layers. For instance, the near-wall reverse flow velocity is comparable to the mean coolant inflow (see Fig. 9), resulting in a friction factor only 15% higher than the steady-flow value at the optimal intermittency condition. Meanwhile, the complex vortical flow pattern greatly reshapes the near-wall temperature distribution (see Fig. 10) and leads to an 121% improvement of the averaged Nusselt number.

In brief, with the acceleration and pulse-on stages preset to match the time scale of cavity vortex development, the deceleration duration of the flow intermittency shall satisfy the criteria of 1.5-groove-pitch transportation distance to maximize the thermal performance enhancement.

Pulse-off Stage

At the pulse-off stage, as the recirculating flow motion gradually dissipates, the heat transfer intensity decays. For all the previous cases, the pulse-off duration is adapted to ensure an identical averaged mass flowrate, for the coolant consumption is one of the critical constraints in practical designs. In comparison to the steady case with Reynolds number of 100, the optimized intermittent case A in Table 1 consumes the same amount of coolant and achieves 121% improvement of the heat transfer performance at the expense of extra 51% pressure loss. Other design prerequisites for the pulse-off durations include maintaining the pressure loss (case B) and the cooling capability (case C). The case B demonstrates that under identical power consumption the flow intermittency enhances the heat transfer by 79%. And the case C suggests that the flow intermittency saves 69% coolant flowrate and 53% power consumption while maintain the same thermal performance. In practical applications, the choice of the pulse-off duration is subject to the specific working conditions and the preferable design prerequisites.

4. Conclusion

The present study numerically compared heat transfer enhancement of intermittent flow in a grooved channel between different velocity profiles. On the basis of the energy buffer mechanism revealed in the previous study, the current work further highlights distinctive flow features that dominate the thermal performance improvement. The main novelty is the introduction of two temporal design criteria that maximize the heat transfer enhancement. One criterion is that the combined duration of acceleration and pulse-on stages shall match the characteristic time for the cavity vortex to fully develop. The fully developed cavity vortex induces intense recirculating flow motion inside the channel and entrains near-wall heated fluids off the boundary. The other is that the duration of the deceleration stage shall complement the transportation distance over a

single flow pulse to be 1.5 groove pitches. The 1.5-groove-pitch transportation distance effectively vents out a great portion of the off-boundary heated fluids and prevents the remnant from being drawn into the grooves. With these two design criteria of flow intermittency satisfied, the duration of the pulse-off stage is adapted to meet different prerequisites in practical applications, such as certain coolant consumption, pressure loss or cooling capability.

Under the same coolant consumption, the optimized intermittent flow increases the averaged wall Nusselt number by 120% and the local *Nu* inside the grooves over 175% in comparison to the steady case. Taking the accompanying pressure loss penalty into account, the overall thermal performance factor is improved by 90%. When the pressure loss is maintained as the design precondition, the heat transfer enhancement still reaches 79%. Further results show that the optimal intermittency pattern saves 69% coolant flowrate and 53% power consumption to achieve the same thermal performance.

Acknowledgements

The authors acknowledge funding by Natural Science Foundation of Shanghai (Grant number 21ZR1428800).

Data Availability Statements

The data that support the findings of this study are available from the corresponding author upon reasonable request.

References

[1] N. Kurtulmuş and B. Sahin, "A review of hydrodynamics and heat transfer through corrugated channels," *Int. Commun. Heat Mass Transf.*, vol. 108, pp. 104307, Nov. 2019. DOI: 10.1016/j.icheatmasstransfer.

[2] G.L. Wang, N. Qian and G.F. Ding, "Heat transfer enhancement in microchannel heat sink with bidirectional rib," *Int. J. Heat Mass Tranf.*, vol. 136, pp. 597-609, Jun. 2019. DOI: 10.1016/j.ijheatmasstransfer.2019.02.018.

[3] G.D. Xia, D.D. Ma, Y.L. Zhai, Y.F. Li, R. Liu and M. Du, "Experimental and numerical study of fluid flow and heat transfer characteristics in microchannel heat sink with complex structure," *Energy Convers. Manag.*, vol. 105, pp. 848-857, Nov. 2015. DOI: 10.1016/j.enconman.2015.08.042.

[4] H.E. Ahmed and M.I. Ahmed, "Optimum thermal design of triangular, trapezoidal and rectangular grooved microchannel heat sinks," *Int. Commun. Heat Mass Transf.*, vol. 66, pp. 47-57, Aug. 2015. DOI: 10.1016/j.icheatmasstransfer.2015.05.009.

[5] J. Liu, G.N. Xie and T.W. Simon, "Turbulent flow and heat transfer enhancement in rectangular channels with novel cylindrical grooves," *Int. J. Heat Mass Tranf.*, vol. 81, pp. 563-577, Feb. 2015. DOI: 10.1016/j.ijheatmasstransfer.2014.10.021.

[6] G.D. Xia, L. Chai, H.Y. Wang, M.Z. Zhou and Z.Z. Cui, "Optimum thermal design of microchannel heat sink with triangular reentrant cavities," *Appl. Therm. Eng.*, vol. 31, no. 6-7, pp. 1208-1219, May. 2011. DOI: 10.1016/j.applthermaleng.2010.12.022.

[7] M. Faghri, K. Javdani and A. Faghri, "Heat transfer with laminar pulsating flow in a pipe," *Lett. Heat Mass Transf.*, vol. 6, no. 4, pp. 259-270, 1979. DOI: 10.1016/0094-4548(79)90013-4.

[8] Z. Jun, Z. Danling, W. Ping and G. Hong, "An experimental study of heat transfer enhancement with a pulsating flow," *Heat Transfer-Asian Research*, vol. 33, no. 5, pp. 279-286, Jun. 2004. DOI: 10.1002/htj.20020.

[9] H.N. Hemida, M.N. Sabry, A. Abdel-Rahim and H. Mansour, "Theoretical analysis of heat transfer in laminar pulsating flow," *Int. J. Heat Mass Tranf.*, vol. 45, no. 8, pp. 1767-1780, Apr. 2002. DOI: S0017-9310(01)00274-5.

[10] R. Siegel and M. Perlmutter, "Heat Transfer for Pulsating Laminar Duct Flow," *J. Heat Transfer*, vol. 84, no. 2, pp. 111-122, 1962. DOI: 10.1115/1.3684307.

[11] J.C. Yu, Z.X. Li and T.S. Zhao, "An analytical study of pulsating laminar heat convection in a circular tube with constant heat flux," *Int. J. Heat Mass Tranf.*, vol. 47, no. 24, pp. 5297-5301, Nov. 2004. DOI: 10.1016/j.ijheatmasstransfer.2004.06.029.

[12] H. Chattopadhyay, F. Durst and S. Ray, "Analysis of heat transfer in simultaneously developing pulsating laminar flow in a pipe with constant wall temperature," *Int. Commun. Heat Mass Transf.*, vol. 33, no. 4, pp. 475-481, Apr. 2006. DOI: 10.1016/j.icheatmasstransfer.2005.12.008.

[13] H.Y. Kim, B.H. Kang and J.M. Hyun, "Heat transfer in the thermally developing region of a pulsating channel flow," *Int. J. Heat Mass Tranf.*, vol. 36, no. 17, pp. 4257-4266, 1993. DOI: 10.1016/0017-9310(93)90088-n.

[14] D.X. Jin, Y.P. Lee and D.Y. Lee, "Effects of the pulsating flow agitation on the heat transfer in a triangular grooved channel," *Int. J. Heat Mass Tranf.*, vol. 50, no. 15-16, pp. 3062-3071, Jun. 2007. DOI: 10.1016/j.ijheatmasstransfer.2006.12.001.

[15] H. Zontul, H. Hamzah, N. Kurtulmuş and B. Şahin, "Investigation of convective heat transfer and flow hydrodynamics in rectangular grooved channels," *Int. Commun. Heat Mass Transf.*, vol. 126, pp. 105366, Jul. 2021. DOI: 10.1016/j.icheatmasstransfer.2021.105366.

[16] H. Zontul and B. Şahin, "Experimental investigation of convective heat transfer performance and hydrodynamics of pulsating flow through the rectangular grooved channel," *Exp. Therm. Fluid Sci.*, vol. 141, pp.110796, Feb. 2023. DOI: 10.1016/j.expthermflusci.2022.110796.
[17] M. Jafari, M. Farhadi and K. Sedighi, "Pulsating flow effects on convection heat transfer in a corrugated channel: A LBM approach," *Int. Commun. Heat Mass Transf.*, vol. 45, pp. 146-154, Jul. 2013. DOI: 10.1016/j.icheatmasstransfer.2013.04.006.
[18] S. Akcay, "Numerical analysis of heat transfer improvement for pulsating flow in a periodic corrugated channel with discrete V-type winglets," *Int. Commun. Heat Mass Transf.*, vol. 134, pp. 105991, May. 2022. DOI: 10.1016/j.icheatmasstransfer.
[19] J. Muñoz-Cámara, D. Crespí-Llorens, J.P. Solano and P. Vicente, "Baffled tubes with superimposed oscillatory flow: Experimental study of the fluid mixing and heat transfer at low net Reynolds numbers," *Exp. Therm. Fluid Sci.*, vol. 123, pp. 1103241 May. 2021. DOI: 10.1016/j.expthermflusci.
[20] Z. Habibi, M. Karami, M. Jarrahi, E. Shirani and H. Peerhossaini, "Some observations on the spatiotemporal orbits structure and heat transfer enhancement in pulsating flow," *Int. J. Therm. Sci.*, vol. 125, pp. 428-439, Mar. 2018. DOI: 10.1016/j.ijthermalsci.2017.12.006.
[21] V.Q. Hoang, T.T. Hoang, C.T. Dinh and F. Plourde, "Large eddy simulation of the turbulence heat and mass transfer of pulsating flow in a V-sharp corrugated channel," *Int. J. Heat Mass Tranf.*, vol. 166, pp. 120720, Feb. 2021. DOI: 10.1016/j.ijheatmasstransfer.
[22] N. Kurtulmuş and B. Sahin, "Experimental investigation of pulsating flow structures and heat transfer characteristics in sinusoidal channels," *Int. J. Mech. Sci.*, vol. 167, pp. 105268, Feb. 2020. DOI: 10.1016/j.ijmecsci.
[23] B. Mehta and S. Khandekar, "Local experimental heat transfer of single-phase pulsating laminar flow in a square mini-channel," *Int. J. Therm. Sci.*, vol. 91, pp. 157-166, May. 2015. DOI: 10.1016/j.ijthermalsci.2015.01.008.
[24] A.M. Bayomy and M.Z. Saghir, "Heat transfer characteristics of aluminum metal foam subjected to a pulsating/steady water flow: Experimental and numerical approach," *Int. J. Heat Mass Tranf.*, vol. 97, pp. 318-336, 2016. DOI: 10.1016/j.ijheatmasstransfer.2016.02.009.
[25] C.S. Wang, T.C. Wei, P.Y. Shen and T.M. Liou, "Lattice Boltzmann study of flow pulsation on heat transfer augmentation in a louvered microchannel heat sink," *Int. J. Heat Mass Tranf.*, vol. 148, pp. 119139, Feb. 2020. DOI: 10.1016/j.ijheatmasstransfer.
[26] C. Xu, S.L. Xu, Z.Y. Wang and D.W. Feng, "Experimental investigation of flow and heat transfer characteristics of pulsating flows driven by wave signals in a microchannel heat sink," *Int. Commun. Heat Mass Transf.*, vol. 125, pp. 105343, Jun. 2021. DOI: 10.1016/j.icheatmasstransfer.
[27] S.W. Chang and T.H. Cheng, "Thermal performance of channel flow with detached and attached pin-fins of hybrid shapes under inlet flow pulsation," *Int. J. Heat Mass Tranf.*, vol. 164, pp. 120554, Jan. 2021. DOI: 10.1016/j.ijheatmasstransfer.
[28] H.S. Sheriff and D.A. Zumbrunnen, "Effect of Flow Pulsations on the Cooling Effectiveness of an Impinging Jet," *J. Heat Transfer*, vol. 116, no. 4, pp. 886-895, 1994. DOI: 10.1115/1.2911463.
[29] J.W. Zhou, Y.G. Wang, G. Middelberg and H. Herwig, "Unsteady jet impingement: Heat transfer on smooth and non-smooth surfaces," *Int. Commun. Heat Mass Transf.*, vol. 36, no. 2, pp. 103-110, 2009. DOI: 10.1016/j.icheatmasstransfer.2008.10.020.
[30] Z.H. Zhang, Q.H. Li, C. Bruecker and Q. Zhang, "Enhanced thermal performance with high-amplitude intermittent impingement cooling," *Int. J. Heat Mass Tranf.*, vol.

185, pp. 122359, Apr. 2022. DOI: 10.1016/j.ijheatmasstransfer.2021.122359.
[31] Z.H. Zhang, Y.J. Tang, Q. Zhang and Z.G. Wang, "Energy Buffer Mechanism for Heat Transfer Enhancement in Grooved Channel Cooling with Flow Intermittency," *Numer. Heat Tr. A-Appl.*, pp. 1-16, Mar. 2023. DOI: 10.1080/10407782.2023.2165581.
[32] N. Kurtulmuş, H. Zontul and B. Sahin, "Heat transfer and flow characteristics in a sinusoidally curved converging-diverging channel," *Int. J. Therm. Sci.*, vol. 148, pp. 106163, Feb. 2020. DOI: 10.1016/j.ijthermalsci.
[33] S. Eiamsa-ard and P. Promvonge, "Numerical study on heat transfer of turbulent channel flow over periodic grooves," *Int. Commun. Heat Mass Transf.*, vol. 35, no. 7, pp. 844-852, Aug. 2008. DOI: 10.1016/j.icheatmasstransfer.2008.03.008.
[34] Q.F. Zhu, H.X. Xia, J.J. Chen, X.M. Zhang, K.P. Chang, H.W. Zhang, H. Wang, J.F. Wan and Y.Y. Jin, "Fluid flow and heat transfer characteristics of microchannel heat sinks with different groove shapes," *Int. J. Therm. Sci.*, vol. 161, pp. Mar. 2021. DOI: 10.1016/j.ijthermalsci.2020.106721.
[35] H.G. Weller, G. Tabor, H. Jasak and C. Fureby, "A tensorial approach to computational continuum mechanics using object-oriented techniques," *CIP*, vol. 12, no. 6, pp. 620-631, Nov-Dec. 1998. DOI: 10.1063/1.168744.
[36] S. Uchida, "The pulsating viscous flow superposed on the steady laminar motion of incompressible fluid in a circular pipe," *ZAMP*, vol. 7, no. 5, pp. 403-422, 1956. DOI: 10.1007/bf01606327.
[37] B. Ünsal, S. Ray, F. Durst and Ö. Ertunç, "Pulsating laminar pipe flows with sinusoidal mass flux variations," *Fluid Dyn. Res.*, vol. 37, no. 5, pp. 317-333, 2005. DOI: 10.1016/j.fluiddyn.2005.06.002.
[38] R.L. Webb, "Performance evaluation criteria for use of enhanced heat transfer surfaces in heat exchanger design," *Int. J. Heat Mass Tranf.*, vol. 24, no. 4, pp. 715-726, 1981. DOI: 10.1016/0017-9310(81)90015-6.

Figure

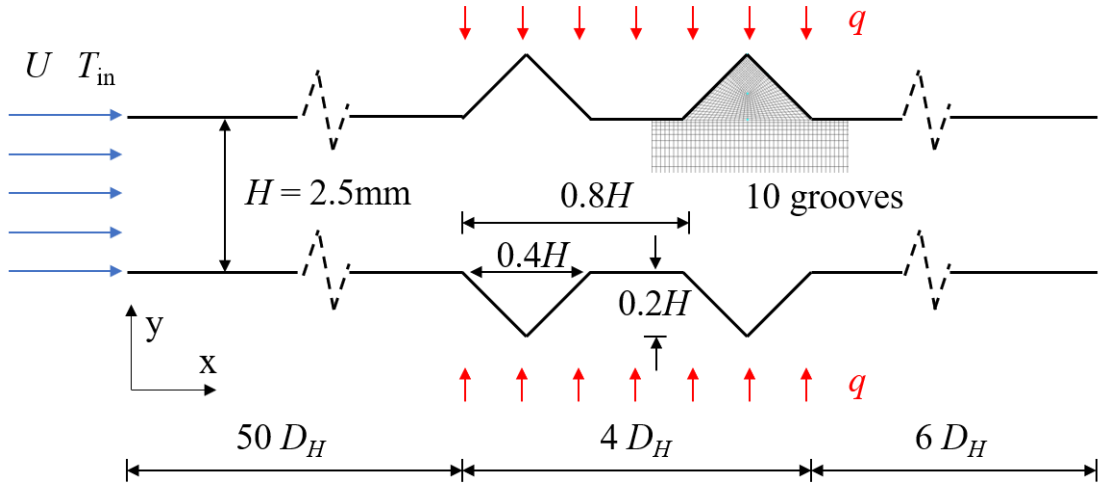

Fig. 1 Geometric dimensions and boundary conditions of the computational domain.

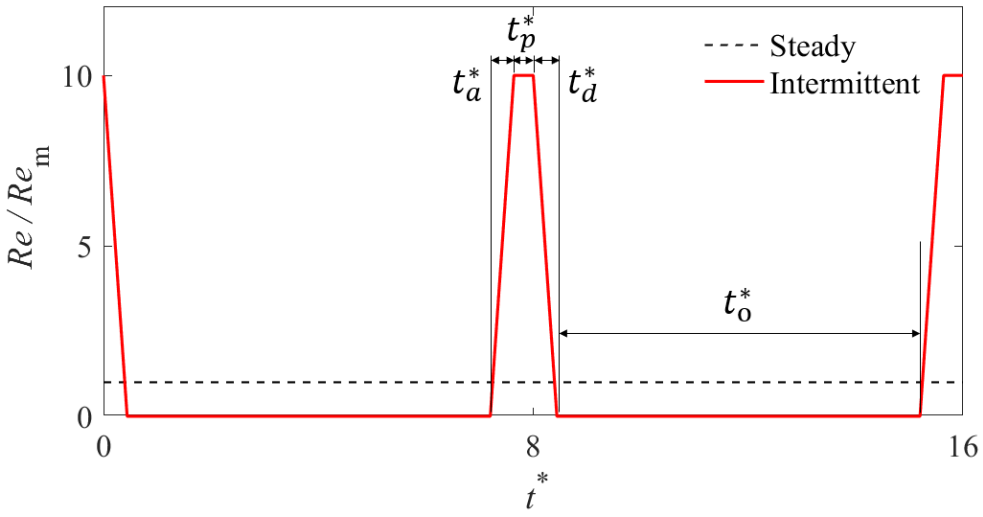

Fig. 2 Intermittent velocity profile

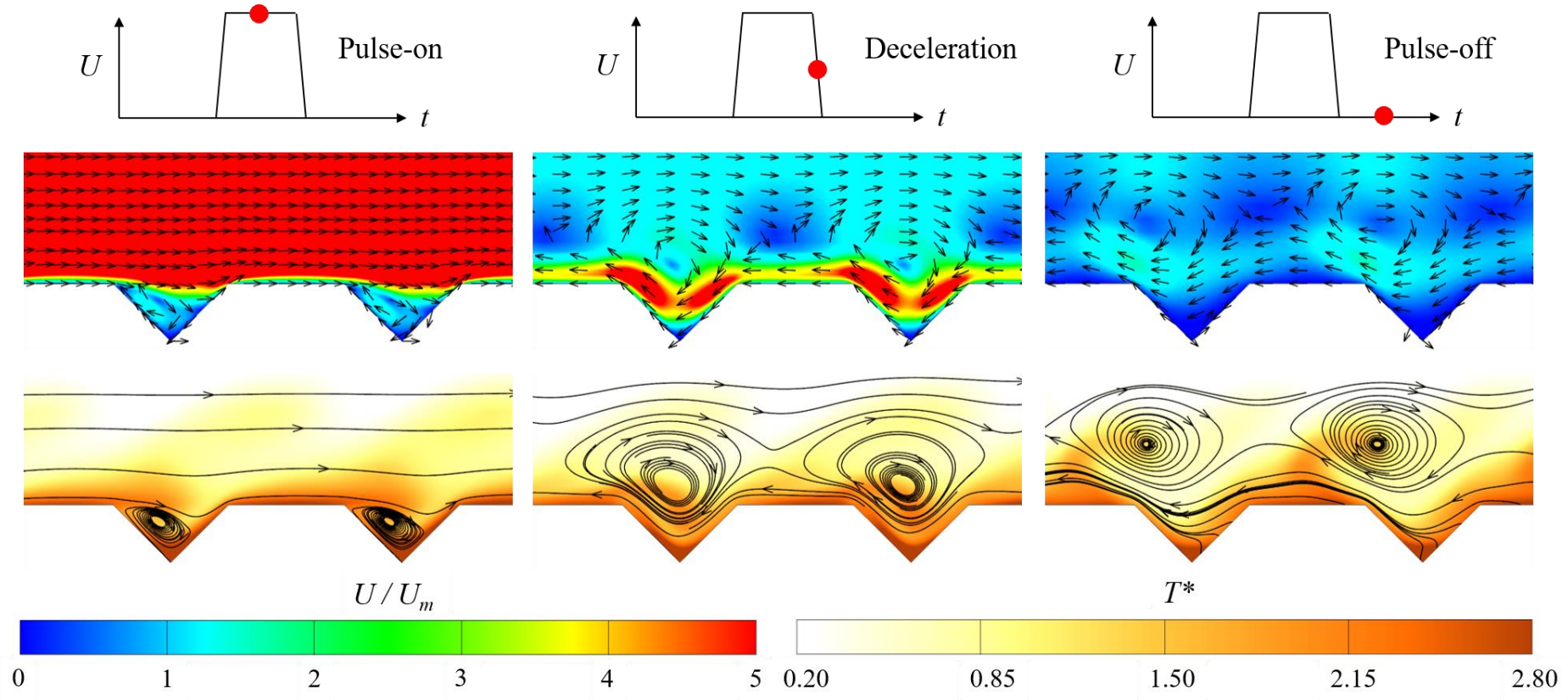

Fig. 3 Velocity contour with streamlines and temperature contour with heatlines at three characteristic time instants. ($Re_m = 100$, $\gamma = 0.9$, $t_a^* = t_d^* = 0.16$)

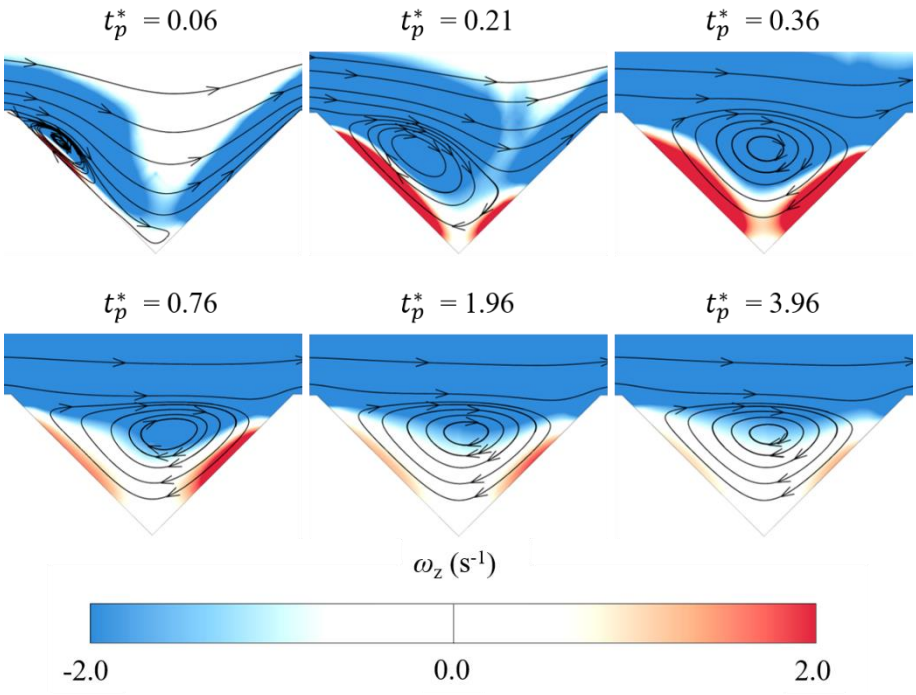

Fig.4 Comparison of Z directional vorticity contours with streamlines zoomed in grooves under various nondimensional pulse-on durations. (Re_m = 100, $t_a^* = t_d^* = 0.04$)

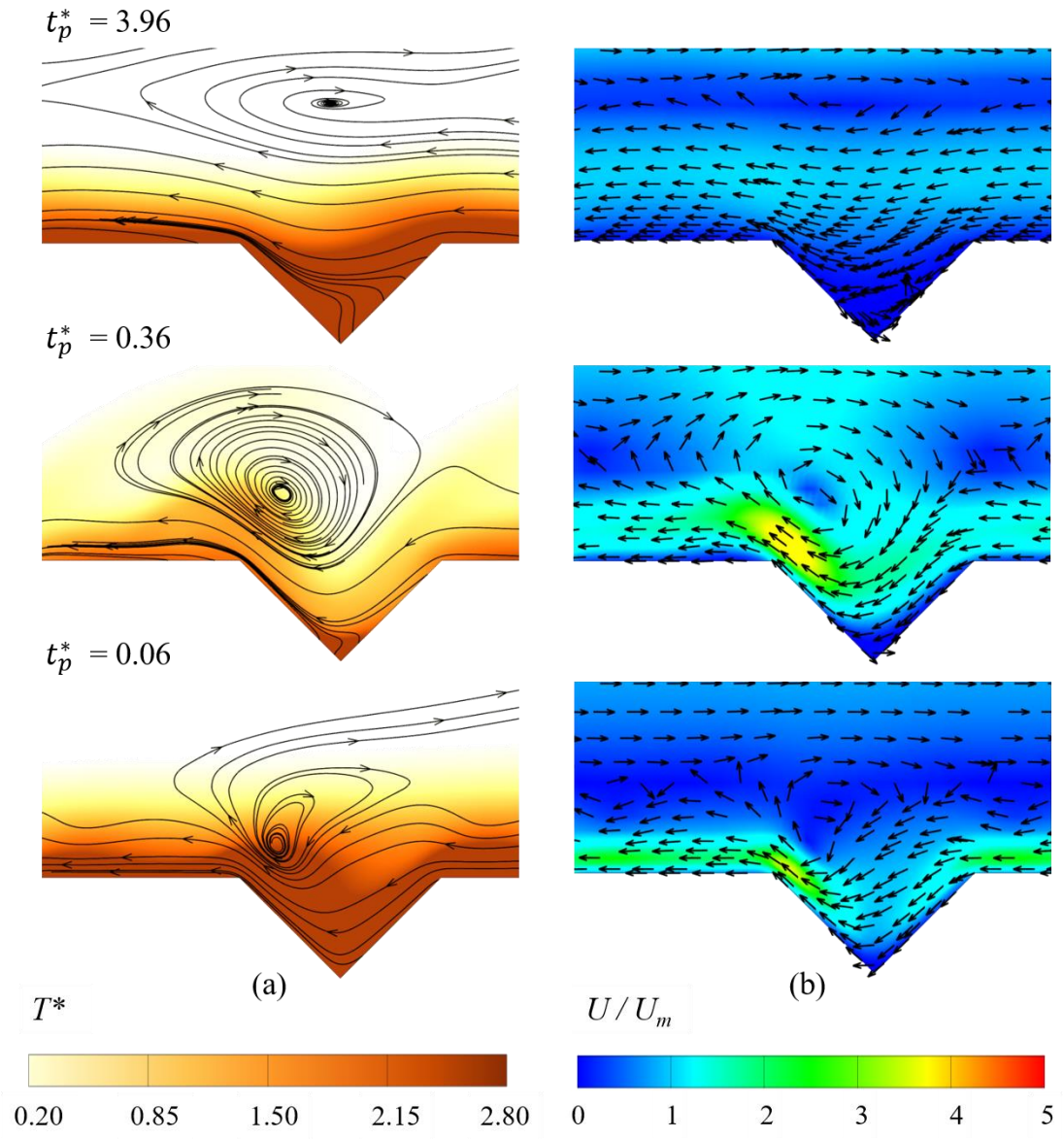

Fig.5 (a) Temperature contour with heatlines; (b) velocity contour with vectors under different dimensionless pulse-on durations at same pulse-off instant. ($Re_m = 100$, $t_a^* = t_d^* = 0.04$, $t_o / t_{period} = 0.1$)

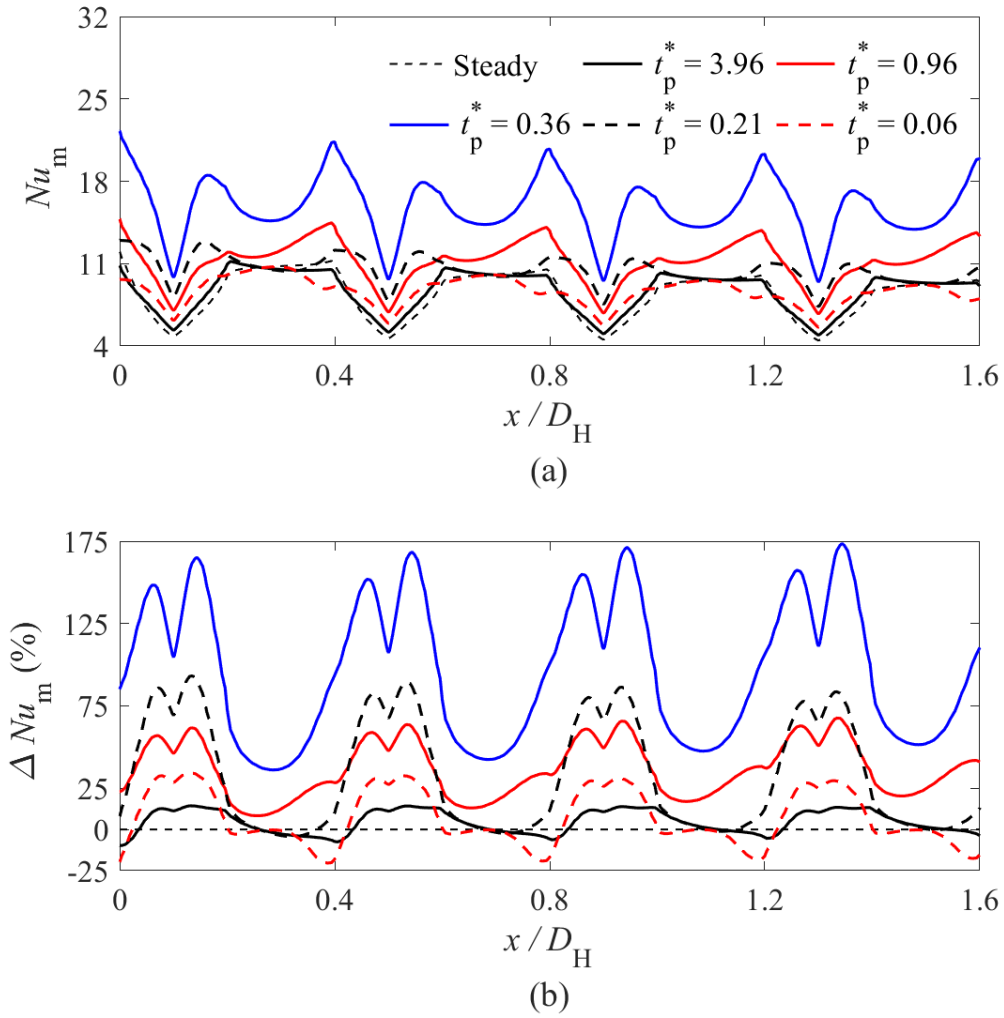

Fig. 6 Spatial variation of time-averaged Nusselt number at different dimensionless pulse-on durations: (a) absolute value; (b) relative percentage difference. (From the fourth to seventh grooves, $Re_m = 100$, $t_a^* = t_d^* = 0.04$)

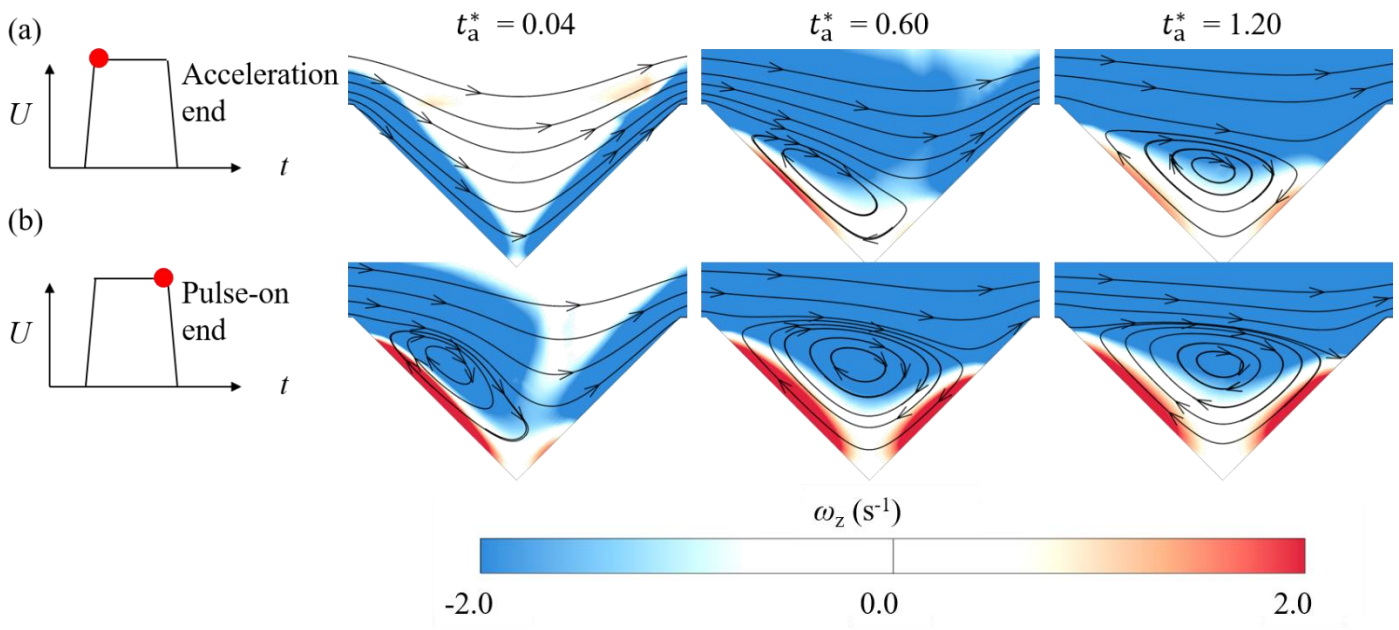

Fig.7 Comparison under different dimensionless acceleration durations of Z directional vorticity contour with streamlines at acceleration end and pulse-on end instants. ($Re_m = 100$, $t_p^* = 0.16, t_d^* = 0.04$)

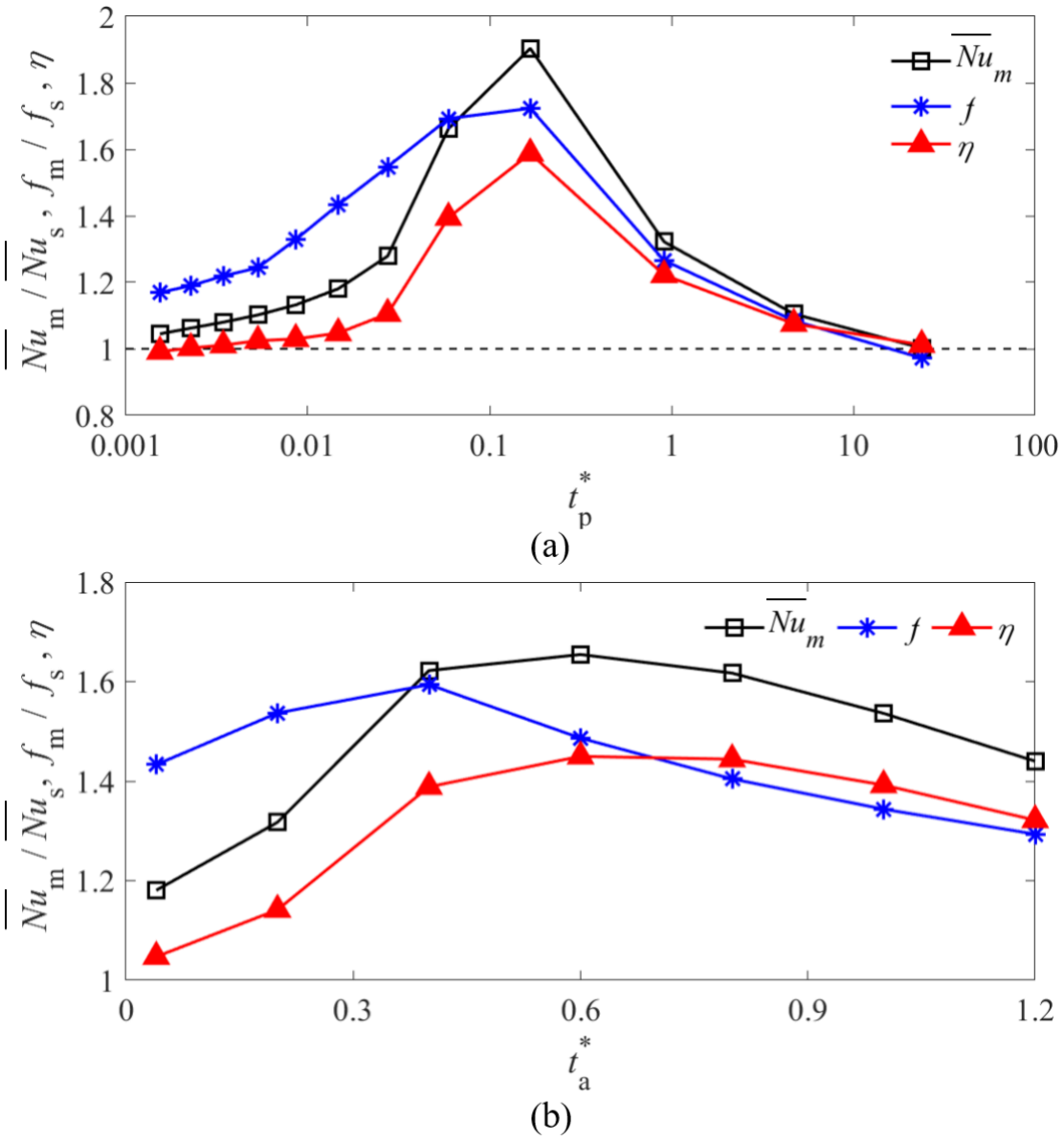

Fig. 8 Comparison of averaged Nusselt number, apparent friction factor and thermal performance factor under (a) different pulse-on durations ($t_a^* = 0.04$); (b) different acceleration durations ($t_p^* = 0.16$). ($Re_m = 100$, $t_d^* = 0.04$)

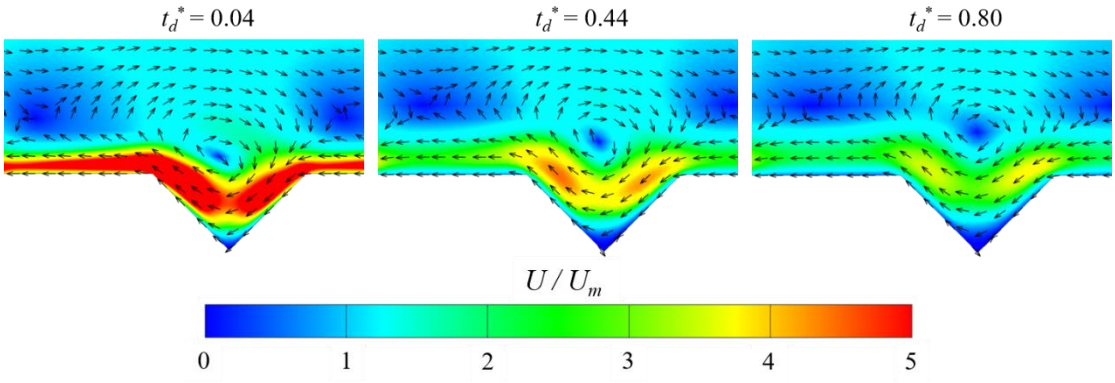

Fig. 9 Velocity contour with vectors under different dimensionless deceleration durations at deceleration end instant. ($Re_m = 100$, $t_p^* = 0.36, t_a^* = 0.04$)

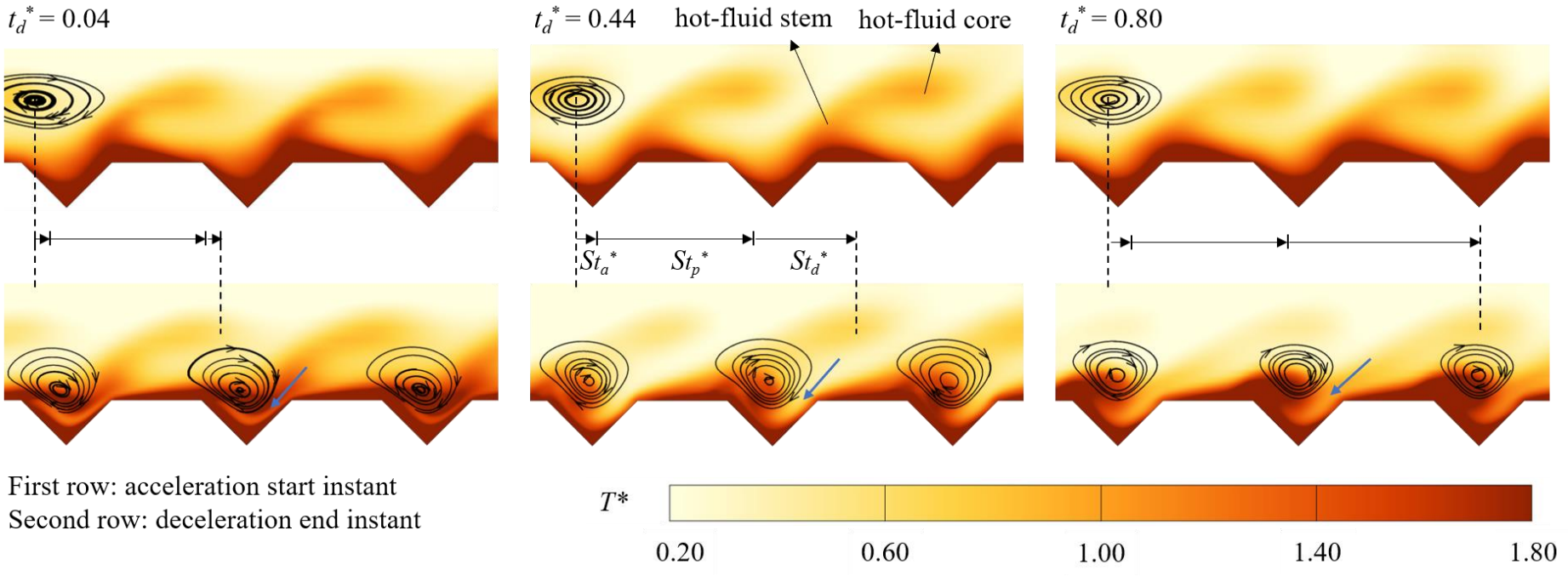

Fig.10 Temperature contour with streamlines under different dimensionless deceleration durations at acceleration start and deceleration end instants. (Re_m = 100, $t_p^* = 0.36, t_a^* = 0.04$)

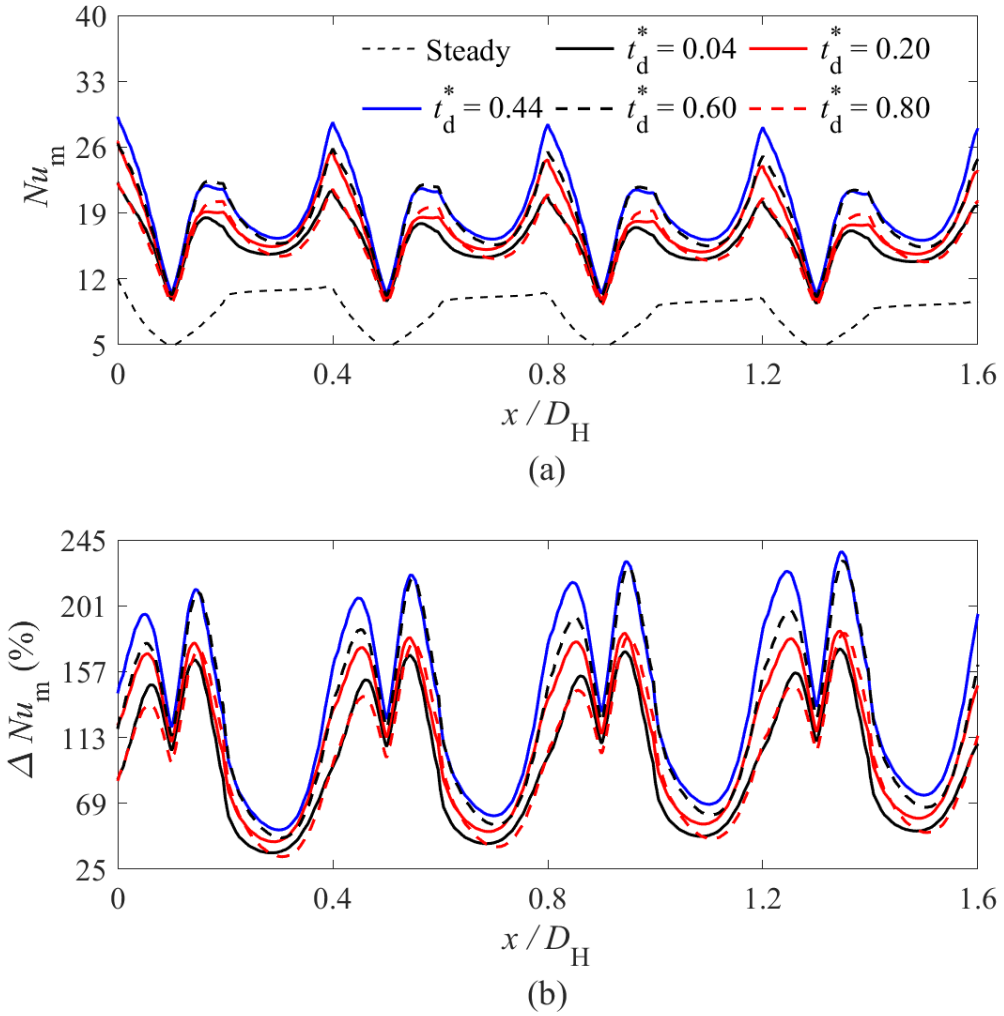

Fig. 11 Spatial variation of time-averaged Nusselt number at different dimensionless deceleration durations: (a) absolute value; (b) relative percentage difference. (From the fourth to seventh grooves, Re_m=100, $t_p^* = 0.36, t_a^* = 0.04$)

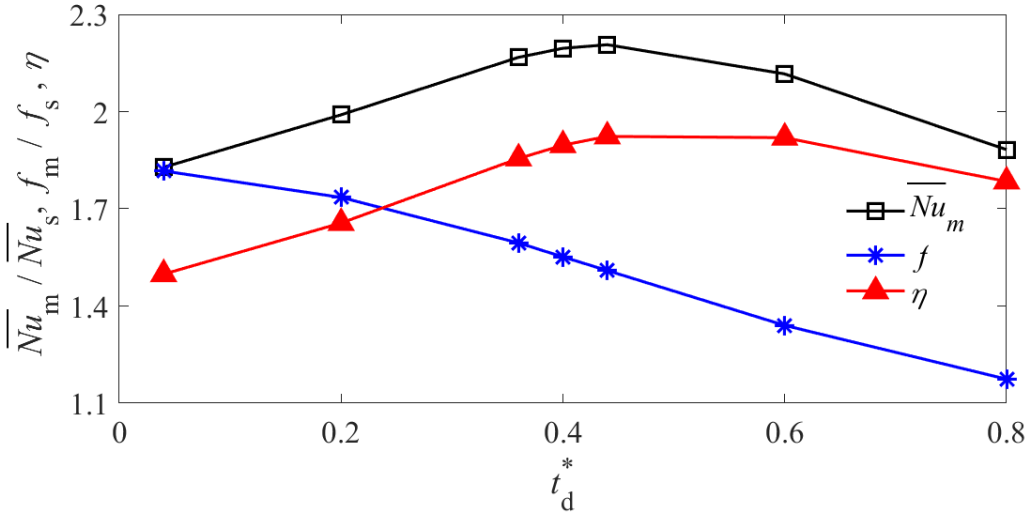

Fig. 12 Comparison of averaged Nusselt number, apparent friction factor and thermal performance factor at different dimensionless deceleration durations. ($Re_m = 100$, $t_p^* = 0.36, t_a^* = 0.04$)

Table

Table 1 Optimized intermittent patterns comparison ($t_a^* = 0.04, t_p^* = 0.36, t_d^* = 0.44$)

Case	A	B	C
Dimensionless pulse-off time t_o^*	5.16	8.44	18.36
Relative mean flow rate (%)	0	-35.35	-68.75
Relative Nusselt number ΔNu_m (%)	120.64	79.20	0
Relative friction factor Δf_m (%)	50.95	0	-52.83
Thermal Performance Factor η	1.9234	1.7920	1.2753